Journal of Structural Geology, Vol. 15, No. 9/10, pp. 1257 to 1271, 1993
Printed in Great Britain

0191-8141/93 $06.00+0.00

Rheology of rocksalt

N. L. CARTER, S. T. HORSEMAN,* J. E. RUSSELL and J. HANDIN

Center for Tectonophysics, Texas A&M University, College Station, TX 77843, U.S.A.

(*Received* 17 *July* 1992; *accepted in revised form* 22 *February* 1993)

Abstract—We review progress in experimental determinations of transient and steady-state flow properties and processes of natural rocksalt aggregates, focusing primarily on results from Avery Island, Louisiana, domal salt. The steady-state flow field—established from constant stress and constant strain-rate tests at temperatures from 50 to 200°C, strain rates from 10^{-5} to 10^{-9} s^{-1} and differential stresses, σ, from 20.7 to 2.5 MPa—has been separated into two flow regimes, each fit by a power-law relation. At the higher stresses and strain rates this relation is

$$\dot{\varepsilon} = 1.6 \times 10^{-4} \exp(-68.1/RT \cdot 10^{-3}) \sigma^{5.3} \quad \text{(A)}$$

for which the pre-exponential constant is expressed in $MPa^{-5.3}$ s^{-1} and the apparent activation energy is in J mol^{-1}. Creep rates predicted by equation (A) do not differ appreciably from those predicted previously. The relatively low stress, low strain-rate data are very well fit by

$$\dot{\varepsilon} = 8.1 \times 10^{-5} \exp(-51.6/RT \cdot 10^{-3}) \sigma^{3.4} \quad \text{(B)}$$

which, at comparable conditions, predicts creep rates higher and equivalent viscosities lower than does equation (A) by two orders of magnitude. The change in behavior from (A) to (B) is ascribed to a change in rate-limiting mechanism from cross-slip of screw dislocations to the climb of edge dislocations in this dry material.

Subgrain formation dominates microstructural development during steady-state flow of salt and, from determinations of average subgrain diameters in crystals from 20 different rocksalt bodies, flow stress levels between 0.6 and 1.4 MPa have been estimated. These values do not bear directly on arguments concerning the nature of forces initiating salt pillow growth because, apparently, evidence relating to the early deformational history has been overprinted. At that stage, fluid-assisted grain boundary diffusional processes might dominate dislocation creep, leading to a linear stress–strain rate mechanical response. Considering buoyancy forces alone, behavior described by equation (B) rather than (A) reduces the relief necessary to initiate pillow growth but a 1000-fold amplification is required to produce stress differences near 1 MPa. That forces other than buoyancy are important is indicated by the occurrence of these same paleostress levels in bedded salts and in shallow offshore concordant intrusions. Differential loading generally provides the most plausible initial driving force for the growth of diapiric salt structures.

INTRODUCTION

ROCKSALT is an invaluable natural resource that forms major deposits in evaporite basins around the globe. In suitable geologic settings, such as rapidly subsiding Gulf-of-Mexico-type basins, salt responds to gravitational forces by flow to form a wide variety of structures, many of which pierce overlying sediments (e.g. Jackson & Talbot 1986). Recent offshore three-dimensional seismic surveys, reflection seismology and other studies show that lateral intrusions from first-generation diapirs may coalesce to form thick concentrations of salt from which may emanate a second generation of salt structures (e.g. Worrall & Snelson 1989, Seni 1991). Laboratory simulations of salt structure evolution using centrifuge techniques (e.g. Talbot & Jackson 1987, Jackson & Talbot 1989) provide insight into the nature and internal structure of diapirs; spectacular sub-horizontal cross-sections through exposed natural diapirs are found in the Great Kavir desert of Iran (Jackson *et al.* 1990). Dynamically scaled physical models of Vendeville & Jackson (1992) suggest that regional extensional faulting and overburden thinning promote diapir growth if the salt supply is adequate and sedimentation is slow; if the salt supply is restricted, diapirs subside and if sedimentation is rapid, growth faulting is promoted. In addition to vertical motions, evidence is mounting in support of large-scale subhorizontal displacements in the form of massifs, nappes and décollements; much of the salt near the Sigsbee Escarpment and elsewhere is now believed to be allochthonous (Worrall & Snelson 1989, Simmons 1992). Salt beneath the sea and sediments in the Gulf of Mexico is in the process of forming a vast and intricate mountain range, three times the size of the Alpine chain and equally complex.

Apart from salt tectonics and related hydrocarbon traps, large and increasing quantities of energy reserves are being stored in large solution-mined caverns in salt domes in the Gulf Coast Basin and elsewhere. Products currently stored in some 2000 underground caverns include brine, petroleum, liquid petroleum products, compressed natural gas and air. Physical properties of domal salt that make it so useful as a storage medium are its very low permeability ($<10^{-20}$ m^2, in the nanodarcy range), very low water content (<100 ppm), high solubility, low density and near incompressibility. Mechanically, rocksalt is as strong as ordinary concrete in the short term but it is weak and ductile in the long term;

*Present address: Intera Information Technologies Ltd, Leicestershire LE13 1AE, U.K.

these strength properties are desirable for mine and cavern construction, for healing discontinuities and for sealing engineered openings.

For analyses both of salt tectonics and geotechnical engineering problems, the flow properties of rocksalt are of fundamental importance. Steady-state flow properties are crucial to both concerns, and transient flow properties are especially important in model predictions of the closure characteristics, stability and behavior of underground openings. Accordingly, we attempt here a brief partial review of the salient information on both transient and steady-state flow properties, primarily of natural rocksalt, and of the corresponding flow processes.

ROCKSALT FLOW PROPERTIES AND PROCESSES

Extensive tests have shown that the total one-dimensional strain of any solid is given by

$$\varepsilon = \varepsilon_e + \varepsilon_p + \varepsilon_t + \varepsilon_s + \varepsilon_a, \quad (1)$$

where ε_e is the elastic strain upon loading, ε_p is the plastic strain produced during loading, ε_t is the transient, primary or decelerating creep strain, ε_s is the secondary or steady-state creep strain and ε_a is the accelerating or tertiary creep strain. Inasmuch as we are interested primarily in large strains, ε_e and ε_p may be neglected although microstructural changes do occur during initial loading in constant stress tests. Accelerating creep and creep-rupture, generally attributed to cracking leading to faulting, are important for geotechnical problems but will not be addressed in this paper. Rather, in this background section, we shall focus upon transient and steady-state flow.

Transient flow

Transient (decelerating) creep of materials at low temperatures ($<0.3\ T_m$; T_m is the melting temperature in K) and stresses high enough to achieve appreciable dislocation mobility generally fits a logarithmic law

$$\varepsilon_t = \alpha \log (1 + \nu t), \quad (2)$$

where α and ν are material constants and t is time. This equation is applicable at room temperature only to materials with high dislocation mobility, such as halite. At higher temperature, two principal types of equations have been applied to transient creep:

$$\varepsilon_t = Bt^m = B_o t^m \sigma^n \exp(-Q/RT) \quad (3)$$

and

$$\varepsilon_t = \varepsilon_T [1 - \exp(-t/\tau)], \quad (4)$$

where B_o, m and n are material constants and Q is the apparent activation energy (J mol^{-1}), R is the universal gas constant (8.32 J mol^{-1}), T is absolute temperature in K, σ is the stress difference, n is the stress exponent, ε_T is the total transient creep strain and τ is a relaxation time.

Carter & Kirby (1978) point out that equation (4) has a firmer basis than equation (3) because: (a) experimental results from a large number of metals and alloys best fit this relationship; (b) it has theoretical support from the observation that the exponential decay law follows a first-order rate equation; (c) equation (3) yields inconsistencies at high and low strains; and (d) the few data for rocks deformed to sufficiently high transient creep strains (>1%) to differentiate between (3) and (4), including halite (Burke 1968), fit (4) very satisfactorily. However, most data for halite and other materials have been analyzed in terms of the power-law transient creep relation (3) and, over most of the conditions employed, the fit is satisfactory. Hansen & Carter (1984) have fitted data for SENM (Salado bedded) salt (Hermann & Lauson 1981a, b) and AI (Avery Island domal) salt both to (3) and to the complete Webster *et al.* (1969) relation. Results for the two different rocksalts, deformed at low temperature in the stress range 6.9–34.5 MPa (Hansen & Carter 1984, fig. 1) indicate that their transient behavior is virtually identical.

More recent treatments of transient flow have attempted to account for damage caused by opening microcracks and voids during dilatation at high stress. Chan *et al.* (1992) consider the macroscopic inelastic strain rate to be comprised of both dislocation and damage-inducing processes. Following Munson & Dawson (1984), the dislocation processes are characterized by a transient component (F) with work-hardening, equilibrium and recovery branches and a steady-state component ($\dot{\varepsilon}s_i$) wherein the strain rate is controlled by three independent, thermally-activated mechanisms, dislocation glide, dislocation climb and an undefined mechanism. The total inelastic macroscopic strain rate is then given by

$$\dot{\varepsilon}_i = F\dot{\varepsilon}s_i + \dot{\varepsilon}^\omega \quad (5)$$

$$\dot{\varepsilon}^\omega = a\omega H(\sigma^\omega)\left[\sinh\left(\frac{b\sigma^\omega H(\sigma^\omega)}{(1-\omega)\mu}\right)\right]^c, \quad (6)$$

where a, b and c are material constants, ω is the damage variable, μ is the shear modulus and H is the Heaviside function with σ^ω as the argument. In this formulation, the inelastic macroscopic strain rate due to microfracturing depends linearly on microcrack density, and hence ω, but it is non-linear with respect to modified stress (Chan *et al.* 1992, equation 14).

Dilatation during transient creep is especially important in evaluating physical characteristics of the disturbed rock zone (DRZ) near the walls of underground openings (Stormont *et al.* 1991). Ratigan *et al.* (1992), using results from 84 tests on Avery Island and Salado salts, have developed a criterion relating damage of rocksalt to the ratio of $\sqrt{J_2}$ to I_1; J_2 is the second stress invariant of the deviatoric stress tensor and I_1 is the first invariant. Damage due to dilatancy increases as $\sqrt{J_2}/0.27\ I_1$ increases above unity; at values lower than unity, crack and pore closure and healing are favored. This criterion was developed for rocksalt at room temperature but it appears also to hold approximately for Asse rocksalt deformed at elevated temperature (Spiers *et al.* 1989, Ratigan *et al.* 1992). There is as yet no quantitative link

between the damage factor, volumetric strain and permeability. However, in laboratory experiments on horizontal cores taken from the 800 m level of the Asse mine, Germany, Peach (1991) found that the permeability decreases from 10^{-18} m^2 to an undisturbed salt value near 10^{-21} m^2 over a distance of 3 m inward from the gallery wall.

We are aware of no systematic study undertaken to determine the load-path dependence of mechanical response and governing micromechanical processes in the transient regime. Such a study is imperative as it would provide fundamental information on: (1) the nature, extent and causes of competing crack opening (dilatancy), healing and microplasticity associated with volumetric strain changes during microstructural evolution to the steady state; (2) evolutionary semi-brittle–ductile behavior that will become a base for future evaluations of effects of pressure, pressure cycling and load paths leading either to steady-state flow or accelerating creep; (3) the long-debated question of whether or not there is a load-path dependence of steady-state micromechanical and mechanical response; and (4) mechanistically-characterized variation of the mechanical response with strain—information essential to refine material models and enhance their predictive capability (e.g. Russell *et al.* 1990, Aubertin *et al.* 1991).

Steady-state flow

An enormous amount of effort has been expended on experimental determinations of the steady-state flow properties and processes of both synthetic and natural rocksalt (e.g. reviews by Carter & Hansen 1983, Senseny *et al.* 1992). Systematic work on natural rocksalt has made use primarily of Asse, Germany, anticlinal salt, Salado, New Mexico, bedded salt and Avery Island (AI), Louisiana, domal salt. AI salt has been used most extensively because of its purity (>99% halite), homogeneity and relatively small (7.5 mm) average crystal size. Experiments on this very dry material have been carried out at elevated temperature and pressure both in the constant stress mode (e.g. Hansen & Carter 1984) and at constant strain rate (Handin *et al.* 1986, Horseman & Handin 1990). Both sets of steady-state data fit well a power-law creep relation (Weertman & Weertman 1970).

$$\dot{\varepsilon}_s = A \exp(-Q_s/RT)\sigma^n, \qquad (7)$$

where the coefficient A (MPa^{-n} s^{-1}) is a slightly temperature-sensitive material constant, and Q_s is the apparent activation energy of the rate-limiting flow mechanism.

Most recently, two experiments on Avery Island salt, deformed at a constant strain rate of 10^{-9} s^{-1} at 50°C (Test 46) and 100°C (Test 47) were terminated after shortening by 11% during a 3.5 year period (Horseman *et al.* 1992). Deformation of these specimens (Fig. 1) is remarkably homogeneous as attested to not only by radial diametral measurements but also by CT (computed tomograph) images that were obtained by translating the specimens through a Technicare Delta 100, 120 kV X-ray Cat Scanner. Images from the centers of both specimens 46 and 47 and are virtually indistinguishable from each other, from undeformed AI, and from any section along the lengths of the deformed samples.

After the CT work, 1 inch discs were cut from the centers of the samples, normal to the cylinder axes, and these were quartered and slabs were cut for further analyses. Doubly-polished thin sections were prepared from each of the specimens (Fig. 1), were immersed in a slightly undersaturated solution of 4 g $FeCl_3$ per l of brine (Urai *et al.* 1987) for 10 s and then rinsed quickly in anhydrous ethyl alcohol, then ether. Figures 2(a) & (b) show the grain boundary structure of specimens 46 (50°C) and 47 (100°C), respectively, as viewed in incident light. For both specimens, grain boundaries are more serrated than are those in the starting material, indicating some mobility during the experiments. There appear to be no appreciable differences in grain boundary migration characteristics between the two experimentally deformed specimens and no other indications of intergranular or intragranular recrystallization. However, subgrains have formed in the experiment at 100°C (Fig. 2b) whereas they are absent in that at 50°C (Fig. 2a).

The nature of the substructure of these specimens was studied in more detail by etching [100] cleavage chips for 30 s in a 4 g $FeCl_3$ per l glacial acetic acid (Mendelson 1961) and then rinsing as described above. Subgrains having an average diameter of 208 μm, enclosing regions with a free dislocation density near 10^7 cm^{-2}, characterize the starting material. Figure 2(c) shows the substructure of specimen 46 (50°C; 10^{-9} s^{-1}). The very high dislocation density and wavy slip bands (dark, irregular N–S-trending bands) are typical of substructural development limited by the cross-slip of screw dislocations; no subgrains have formed in this specimen. In contrast, well-developed subgrains having an average diameter of 28 μm, enclosing regions of low free dislocation density, characterize specimen 47 (100°C, 10^{-9} s^{-1}; Fig. 2d). In addition to the cross-slip of screw dislocation segments, well-formed subgrains require extensive climb of edge dislocations by atom and vacancy diffusion and this process is generally considered to limit the strain rate during development of this type of substructure. C. J. Peach & C. J. Spiers (personal communication, November 1992) examined specimen 47 after irradiation (Urai *et al.* 1986) and confirmed the dominance of subgrains and absence of significant recrystallization.

Salt in domes of the Gulf Coast and Interior basins are typically very dry (<100 ppm H_2O by weight; Knauth & Kumar 1981). Samples of the Avery Island starting material and from the central discs cut from specimens 46 and 47 were sent to L. Paul Knauth for mass spectrometric determination of water content. The starting material was 17 ppm H_2O by weight, specimen 46 (at 50°C), was 10 ppm, and specimen 47 (at 100°C), was 89 ppm H_2O (Table 1). Two additional pieces of specimen 47 were subsequently analyzed for confirmation; one from the center and the other from the end of the specimen contain 91 and 143 ppm H_2O by weight,

Table 1. Avery Island Salt: water content

Sample No.	Bulk wt% H_2O (mass spectrometry)*	Crystal wt% H_2O (infrared spectroscopy)† Integrated Absorbance (cm^{-2})	wt% H_2O
AI 85 (D)			
Undeformed	0.0017	1. 20	
		2. 13	
Average	0.0017	16.5	0.00043
AI 46B			
50°C, 10^{-9} s^{-1}	0.0010	B_1 15	
		B_2 21	
		B_3 29	
Average	0.0010	21.7	0.000565
AI 47B			
100°C, 10^{-9} s^{-1}	0.0089	B_1 8.4	
	0.0143	B_2 5.0	
	0.0091	B_3 11.3	
Average	0.0177	8.2	0.000215

*Analyses by L. Paul Knauth, Arizona State University, May and July 1992.
†Integrated absorbance obtained by Andreas K. Kronenberg, Texas A&M University, June 1992. H_2O content calculated using Stolper's (1982) value for wt fraction H_2O in glass (integrated absorbance × 2.61 × 10^{-7}; Kronenberg personal communication, June 1992).

respectively (L. P. Knauth personal communication, July 1992). Thus, specimen 47 contains an average of 108 ppm H_2O; still very dry but much damper than the other two samples (Table 1). However, A. K. Kronenberg (personal communication, July 1992) found little difference in the water content of grain interiors from the three specimens as determined by infrared spectroscopy of cleavage chips. Integrated absorbances range from an average of 8.0 cm^{-2} for specimen 47 through 16.5 cm^{-2} for the starting material to 21.7 cm^{-2} for specimen 46 (Table 1). As reliable calibrations of molar absorptivity of H_2O in NaCl are not available, we use Stolper's (1982) calibration for molar absorptivity of H_2O in silica glass to estimate intragranular water content. On the basis of this assumption, these absorbance values correspond approximately to from 2.2 ppm H_2O by weight for crystals from specimen 47, to 5.7 ppm for specimen 46. While the mass spectrometric determinations are more accurate, they represent bulk concentrations, not that within individual crystals. Therefore, the relatively high H_2O content of specimen 47 probably reflects water concentrated at grain boundaries; apparently, this has had little effect on microstructural development.

Stress–strain curves for these specimens (Fig. 3) show that specimen 47 (100°C) was in the steady state at 2% strain, whereas specimen 46 (50°C) is still work-hardening slightly at 11% strain (Horseman *et al.* 1992). All constant strain-rate, steady-state data (Table 2) were fitted, by weighted non-linear least-squares regression, to the power relation (7);

$$\dot{\varepsilon} = 6.4 \times 10^{-5} \exp(-69.2/RT \cdot 10^{-3})\sigma^{5.9}. \quad (8)$$

While the fit (Fig. 4 and Table 3) is satisfactory, test point 47 falls about 3 MPa below the predicted 100°C

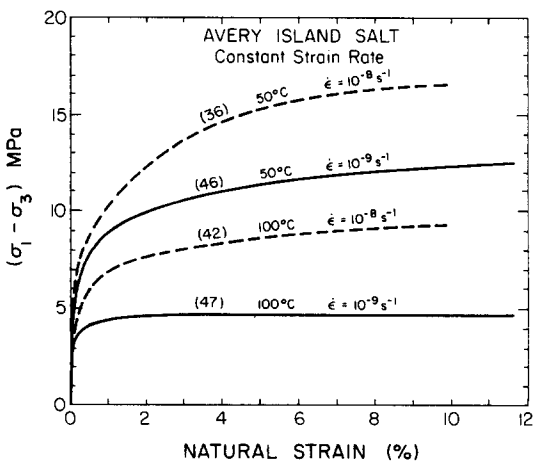

Fig. 3. Stress–strain curves for specimens 46 and 47, deformed at a strain rate of 10^{-9} s^{-1} over a 3.5 year period. Earlier results of Horseman & Handin (1990) at 10^{-8} s^{-1} (dashed curves) are shown for comparison.

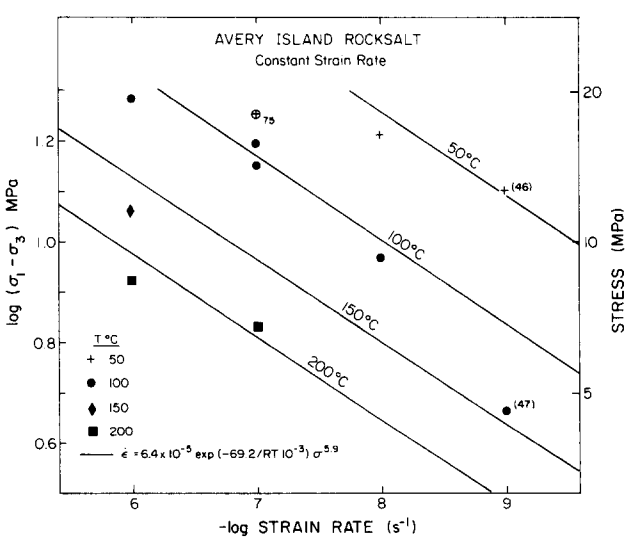

Fig. 4. −Log strain rate vs log stress plot of all steady-state constant strain rate data for Avery Island (AI) salt at 10% strain (Table 2). Isotherms are generated from weighted non-linear least-squares regression equation (8) in lower left (Table 3).

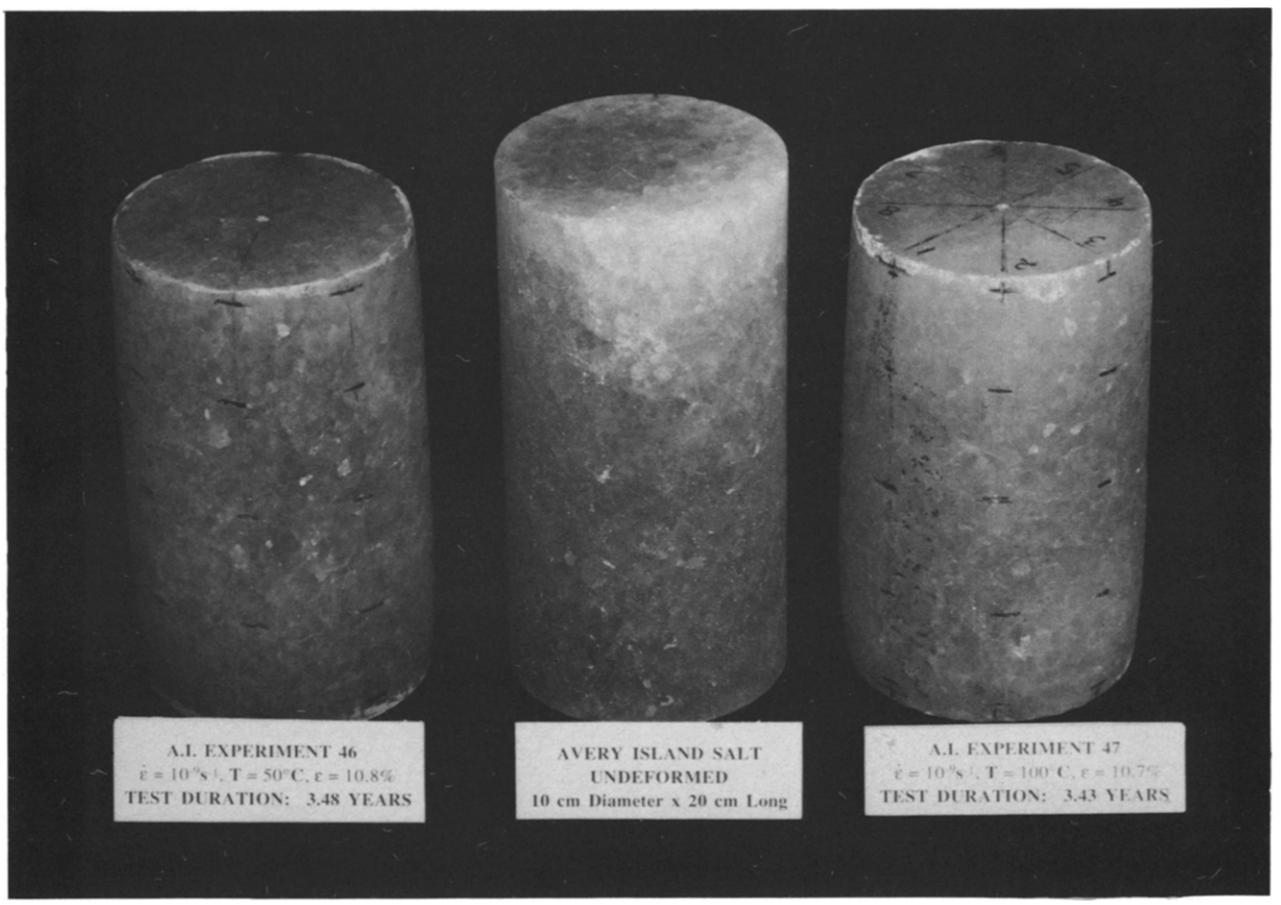

Fig. 1. Photograph of 10 cm diameter by 20 cm long sample of Avery Island salt starting material (center) flanked by tests 46 (left, 50°C) and 47 (right, 100°C).

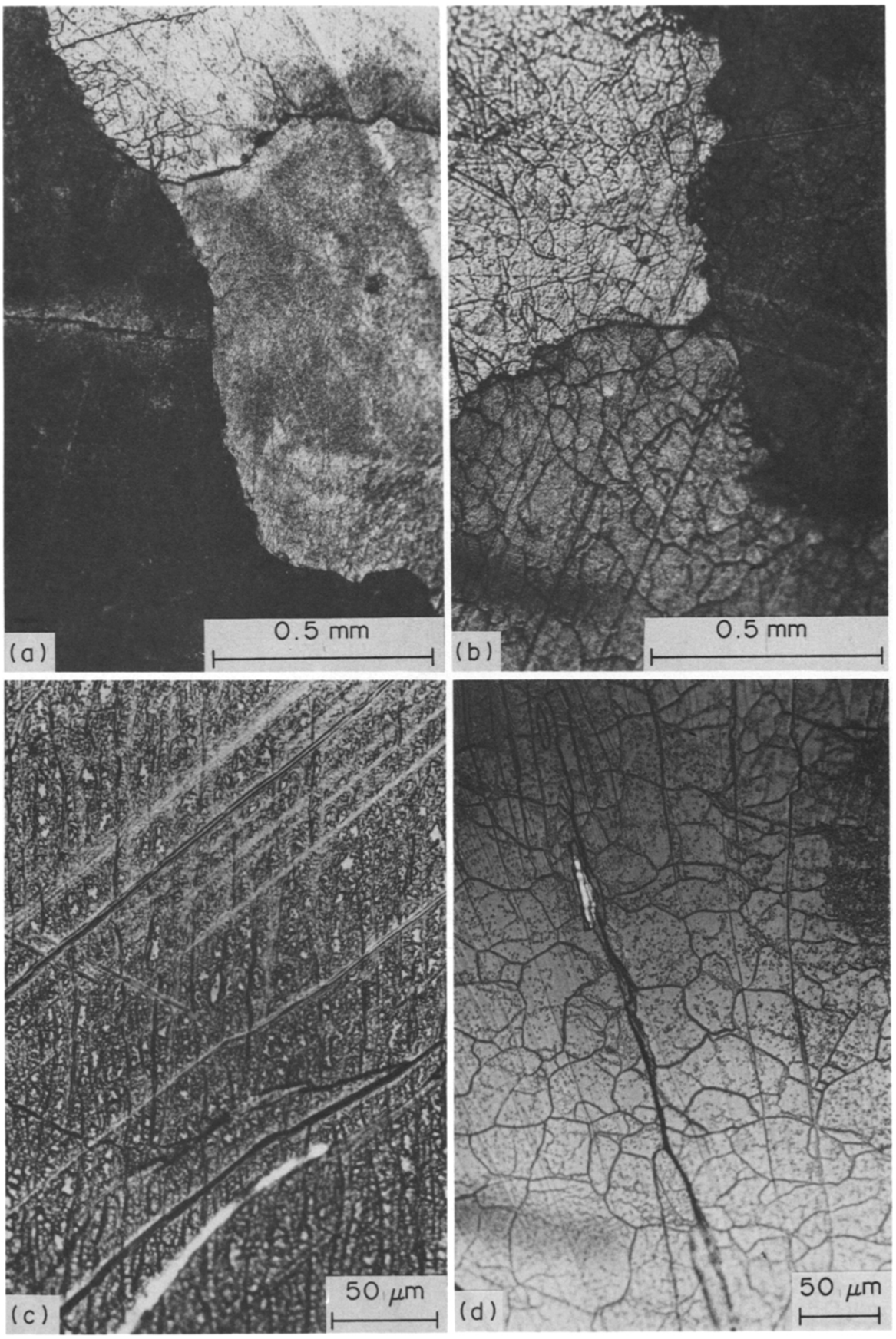

Fig. 2. Photomicrographs taken in incident light of etched surfaces (a & b) and cleavage chips from specimens 46 (a & c; 50°C, 10^{-9} s^{-1}) and 47 (b & d; 100°C, 10^{-9} s^{-1}). (a) Specimen 46; grain boundary migration is indicated by the serrated nature of the boundaries. (b) Specimen 47; boundary migration and development of networks of subgrains. (c) Specimen 46; etched cleavage chip showing high etch pit (dislocation) density and wavy slip bands (N–S-trending, dark irregular bands) indicative of extensive cross-slip (NE-trending bands are cleavage steps). (d) Specimen 47; etched cleavage chip showing subgrains, whose dark irregular boundaries enclose regions of low free dislocation density.

Table 2. Avery Island steady-state data

Temp. (°C)	$(\sigma_1 - \sigma_3$ (MPa)	$\dot{\varepsilon}_s$ (s^{-1})	Test No.	Source
Constant strain-rate tests				
50	16.4	1.00×10^{-8}	36-D	Horseman & Handin (1990)
50	12.3	1.00×10^{-9}	46-D	Horseman *et al.* (1992)
75	17.9	1.00×10^{-7}	33-D	Horseman & Handin (1990)
100	18.9	1.00×10^{-6}	35-D	Horseman & Handin (1990)
100	14.1	1.00×10^{-7}	34-D	Horseman & Handin (1990)
100	15.6	1.00×10^{-7}	45-C	Horseman & Handin (1990)
100	9.4	1.00×10^{-8}	42-D	Horseman & Handin (1990)
100	4.7	1.00×10^{-9}	47-D	Horseman *et al.* (1992)
150	11.7	1.00×10^{-6}	20-B	Handin *et al.* (1986)
200	8.6	1.00×10^{-6}	9-C	Handin *et al.* (1986)
200	6.8	1.00×10^{-7}	43-C	Horseman & Handin (1990)
Constant stress tests				
75	10.0	2.32×10^{-9}		Senseny (1988)
80	20.7	1.12×10^{-7}	AI4B-1A	Hansen & Mellegard (1980)
100	5.0	1.20×10^{-9}		Senseny (1988)
100	7.5	4.48×10^{-9}		Senseny (1988)
100	15.0	6.75×10^{-8}		Senseny (1988)
100	5.0	1.25×10^{-9}	100-11	Hansen & Carter (1984)
100	18.1	1.74×10^{-7}	100-12	Hansen & Carter (1984)
100	20.7	8.28×10^{-7}	100-13	Hansen & Carter (1984)
100	10.3	8.15×10^{-9}	100-15	Hansen & Carter (1984)
100	15.5	8.07×10^{-8}	100-16	Hansen & Carter (1984)
100	15.5	7.71×10^{-8}	100-18	Hansen & Carter (1984)
112	10.3	2.84×10^{-8}	100-1	Hansen & Carter (1984)
112	20.7	1.68×10^{-6}	100-3	Hansen & Carter (1984)
112	10.3	5.42×10^{-8}	100-4	Hansen & Carter (1984)
112	10.3	5.30×10^{-8}	100-6	Hansen & Carter (1984)
112	10.3	4.76×10^{-8}	100-8	Hansen & Carter (1984)
170	10.3	3.99×10^{-7}	150-1	Hansen & Carter (1984)
200	10.3	1.17×10^{-6}	200-1	Hansen & Carter (1984)
200	10.3	1.49×10^{-6}	200-2	Hansen & Carter (1984)
200	6.9	2.80×10^{-7}	200-3	Hansen & Carter (1984)
200	6.9	1.77×10^{-7}	200-4	Hansen & Carter (1984)
200	5.5	7.20×10^{-8}	200-5	Hansen & Carter (1984)
200	5.5	5.95×10^{-8}	200-6	Hansen & Carter (1984)
200	2.5	3.40×10^{-9}	200-7	Hansen & Carter (1984)
200	5.0	4.16×10^{-8}		Senseny (1988)
200	7.5	1.33×10^{-7}		Senseny (1988)
200	10.3	1.76×10^{-6}		Senseny (1988)

isotherm. The activation energy is near that found for steady state flow of other rocksalts but the stress exponent is higher than the 4.5 value previously obtained for creep of Avery Island salt (Hansen & Carter 1984). However, n values >5 have been observed in steady-state data sets for Asse, W. Hackberry, Bryan Mound and Salina domal and anticlinal salts and for Salado and Palo Duro Units 4 and 5 bedded salt (Wawersik & Zeuch 1986, Hansen 1987, Senseny 1988, Skrotski & Haasen 1988, Wawersik 1988). At a strain rate of 10^{-6} (Fig. 4), data points at all three temperatures fall below the isotherms suggesting an underestimate of the steady-state stress which then leads to an overestimate of the stress exponent.

The initial fit of 18 constant-stress, steady-state data points by Carter & Hansen (1983) and Hansen & Carter (1984) (deviation corrected by Handin *et al.* 1986) (see Table 3) gave

$$\dot{\varepsilon} = 7.6 \times 10^{-4} \exp(-66.5/RT \cdot 10^{-3})\sigma^{4.5}. \quad (9)$$

A refit of these data, adding six subsequent data points from Senseny (1988) and three others (Table 2), gives

$$\dot{\varepsilon} = 2.6 \times 10^{-4} \exp(-61.6/RT \cdot 10^{-3})\sigma^{4.3}. \quad (10)$$

The fit is shown in Fig. 5 and the results are listed in Table 3. Notice that the three data points at the lowest strain rate fall well below the corresponding isotherms.

Table 3. Parameter estimates for steady-state flow non-linear weighted regression—$\dot{\varepsilon} = A \exp(-Q/RT)\,\sigma^n$

Data (Table 1)	No. of data	A	1 SD	Q/R	1 SD	n	1 SD
1. Constant strain rate	11	6.36×10^{-5}	9.75×10^{-5}	8315	774	5.93	0.77
2. Constant stress	27	2.62×10^{-4}	1.92×10^{-4}	7412	393	4.31	0.28
3. Constant strain rate + constant stress	38	2.02×10^{-4}	1.29×10^{-4}	7498	338	4.52	0.28
4. Constant strain rate + constant stress (low $\dot{\varepsilon}$, σ)	10	8.12×10^{-5}	2.66×10^{-5}	6206	144	3.42	0.11
5. Constant strain rate + constant stress (high $\dot{\varepsilon}$, σ)	28	1.57×10^{-4}	1.29×10^{-4}	8191	434	5.34	0.39

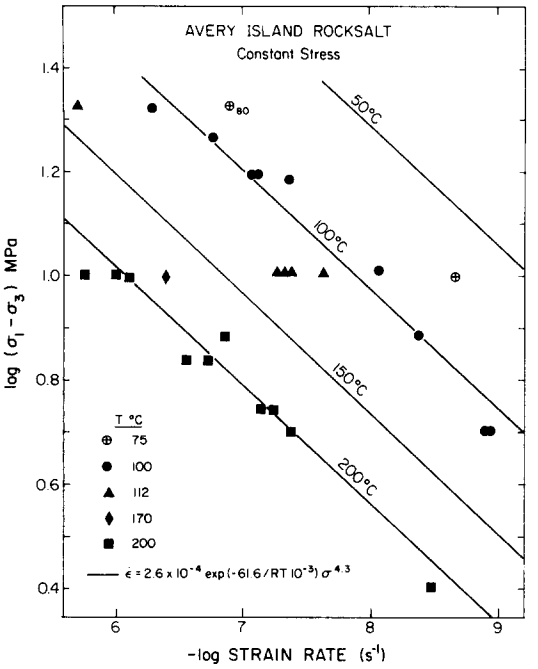

Fig. 5. −Log strain rate vs log stress plot of all steady-state data for AI salt deformed at constant stress (Table 2). Isotherms are generated from weighted non-linear least-squares regression equation (10) in lower left (Table 3).

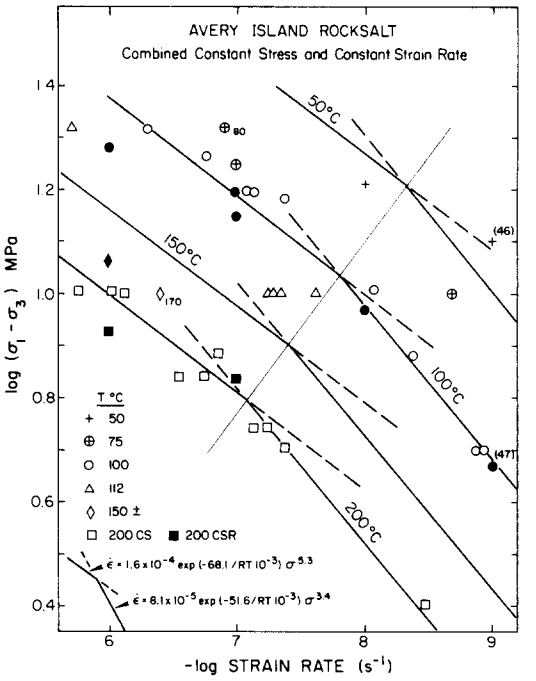

Fig. 7. −Log strain rate vs log stress plot of data shown in Fig. 6, divided into high stress and strain rate and low stress and strain rate regimes with corresponding fits (equations 12 and 13) shown in lower left (Table 3).

Next, the constant stress and strain-rate data were combined (Fig. 6) and refit (Table 3)

$$\dot{\varepsilon}_s = 2.0 \times 10^{-4} \exp(-62.3/RT \cdot 10^{-3})\sigma^{4.5}. \quad (11)$$

This result (Horseman *et al.* 1992) is not appreciably different from the initial fit by Hansen & Carter (1984) as given by (9) and the subsequent fit with additional creep data as reflected by (10). Evidently, the 27 creep data points swamp the 11 constant strain-rate data. Again, noting in Fig. 6 that four data points at the lowest strain rates fall significantly below the 100 and 200°C isotherms, Horseman *et al.* (1992) refit 10 low stress and low strain-rate data points (five at 100°C, $\dot{\varepsilon} \leq 10^{-8}\,s^{-1}$, five at 200°C, $\dot{\varepsilon} \leq 10^{-7}\,s^{-1}$) and then the remainder separately to equation (7). The result is listed in Table 3 and shown in Fig. 7 where it is apparent that the fit to the low stress, low strain-rate data is excellent. The flow law for this data set is

$$\dot{\varepsilon} = 8.1 \times 10^{-5} \exp(-51.6/RT \cdot 10^{-3})\sigma^{3.4} \quad (12)$$

and that for the remaining relatively high stress, high strain-rate data is

$$\dot{\varepsilon} = 1.6 \times 10^{-4} \exp(-68.1/RT \cdot 10^{-3})\sigma^{5.3}. \quad (13)$$

These results suggest that there is a change in behavior of Avery Island rocksalt near 200°C, $10^{-7}\,s^{-1}$ and 100°C, $10^{-8}\,s^{-1}$. This change has not occurred in test 46 (50°C, $10^{-9}\,s^{-1}$) and hence the boundary between the two flow regimes must be deflected toward lower strain rates (to the right in Fig. 7).

The change in behavior indicated must result from a change in rate-controlling mechanism, perhaps from cross-slip of screw dislocations at relatively high stress and strain rate (Wawersik & Zeuch 1986, Skrotski & Haasen 1988, Wawersik 1988) to climb of edge dislocations at the lower stresses and strain rates (e.g. Carter & Hansen 1983, Horseman *et al.* 1992, Senseny *et al.* 1992). On the basis of activation analyses of results from constant stress experiments on Asse and Salado salts, in the temperature range 40–160°C, stress range 8.3–16.3 MPa and strain rates from 10^{-6} to $10^{-9}\,s^{-1}$, Wawersik & Zeuch (1986) and Wawersik (1988) suggested that cross-

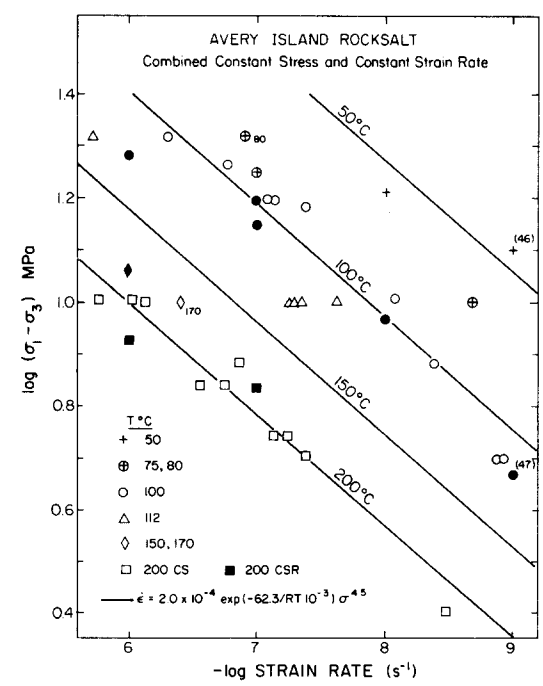

Fig. 6. −Log strain rate vs log stress plot of combined constant stress and constant strain-rate data (Table 2). Isotherms are generated from weighted non-linear least-squares regression equation (11) in lower left (Table 3).

slip has controlled the creep rate in those experiments. Skrotski & Haasen (1988) arrived at a similar conclusion following their analysis of activation volumes and of the temperature dependence of the stress exponent, n, of combined single crystal and synthetic and natural polycrystal data. However, the most compelling argument in favor of cross-slip controlled steady-state creep at elevated temperature and relatively high stress comes from detailed examination of the microstructures. Wavy slip bands (Wawersik & Zeuch 1984, Senseny *et al.* 1992) of the type shown in Fig. 2(c) provide excellent evidence for extensive cross-slip of screw dislocations. The waviness results from irregular bridging of parallel {110} slip planes by screw dislocations that have moved for short distances on {100} and {111} planes.

Evolution of the microstructure from the dislocation-glide type (Fig. 2c) to the dislocation-creep type (Fig. 2d) requires extensive diffusion of vacancies or atoms to the cores of edge dislocations. These dislocations may then surmount obstacles to slip by climbing out of their slip plane to another on which they may glide to stable walls of dislocations forming subgrain boundaries. This process, together with recombination and annihilation of dislocations, and hence reduction of free dislocation densities within subgrains, results in large reductions in the strain energy of the crystals. Since diffusion, regardless of path or atomic species, is inherently a slow process, especially at these low temperatures, it is generally considered to be the rate-limiting mechanism during formation of a subgrain-dominated substructure such as that shown in Fig. 2(d). While it is difficult, on any basis, to ascertain the physical conditions for the transition from cross-slip to climb control of the strain rate, we suggest that the boundary shown in Fig. 7 represents the best approximation to date.

Recent discussions of the phenomenology of steady-state flow in face-centered cubic metals also emphasize the importance of contributions to the creep rate of two or more mechanisms operating in parallel. Blum *et al.* (1989), on the basis of stress reduction tests on aluminum at elevated temperature, suggest that steady-state flow results from a balance between recovery at hard (creep resistant) subgrain boundaries and glide in soft subgrain interiors, these two mechanisms being coupled by internal stresses. Stone (1991) has developed a micromechanical model, based on self-similarity of subgrain diameters, whereby steady-state flow properties are governed solely by the subgrains generated during the deformation. In this model, athermal dislocation glide and diffusion-controlled subgrain-boundary migration compete in each subgrain. For large subgrains, glide, involving cross-slip, controls the flow stress and for small ones, dynamic recovery associated with subgrain boundary migration ($n = 3$ at low temperature) dominates; the volume fraction of each mechanism is partitioned such that constant stress and strain rate are maintained.

Subgrain size vs stress

Subgrains form the dominant microstructures in all naturally deformed intrusive rocksalt structures examined to date. Raleigh & Kirby (1970) first applied the subgrain size–stress paleopiezometer (Servi & Grant 1951) to olivine-rich rocks and Poirier (1972) first applied it to halite crystals. Since then, this method has been shown to apply to many materials deforming in the steady-state flow regime (e.g. reviews by Takeuchi & Argon 1976, Carter & Tsenn 1987). Subgrain size is inversely related to stress, virtually independent of all other variables, by

$$D = k\sigma^{-m}, \tag{14}$$

where k is a material constant, σ is the stress difference and m is a constant that may range between 0.5 and 1.5 but most commonly has a value near unity. An expression somewhat similar to (14) is obtained for grain size of dynamically recrystallized salt crystals (Guillope & Poirier 1979). Although the technique is not yet fully developed, it might be useful for highly deformed dry salt (Senseny *et al.* 1992) and for salt deformed in the presence of excess water (Spiers *et al.* 1986, Urai *et al.* 1986, 1987). Free dislocation density is directly related to the steady-state stress difference raised to a power ranging from 0.33 to 2.2 (Takeuchi & Argon 1976) but this method must be used with caution because of the ease with which dislocations are introduced in salt (Carter & Hansen 1983, Hansen 1987, Senseny *et al.* 1992). Beeman & Kohlstedt (1988), from experiments on natural and synthetic single crystals, found the power on stress to be 1.3 for both materials. As applied to Lansing, New York salt, obtained near the wall of a mine opening, *in situ* stresses ranging from 10 to 30 MPa are inferred; these high values are attributed to disturbances associated with the excavation.

The steady-state stress–subgrain size relation for experimentally deformed Avery Island salt (Carter *et al.* 1982) is

$$D(\mu\text{m}) = 190\sigma^{-1.0}\,(\text{MPa}). \tag{15}$$

Subsequently, Hansen (1987), combining data from Avery Island, Salina and Palo Duro units 4 and 5, found the best fit to be

$$D(\mu\text{m}) = 178\sigma^{-0.97}. \tag{16}$$

Table 4 shows individual and combined fits to all available data for experimentally deformed natural rocksalt. We suggest use of the Avery Island combined constant stress and constant strain-rate result (Fig. 8)

$$D(\mu\text{m}) = 214\sigma^{-1.15} \tag{17}$$

which differs little from the initial result (15) and even less from that for all tests combined (Table 4); the lower correlation coefficient of the latter reflects the larger scatter in Palo Duro unit 5 data (Hansen 1987).

Equation (17) has been used to estimate steady-state flow stresses in rocksalt from three provinces associated with evolution of the Gulf of Mexico as well as for bedded and anticlinal salts elsewhere (Table 5). The salt structures listed under coastal and Interior Basins are domal salts. The large numbers of observations for Big Hill and Bryan Mound (Table 5) result from combining

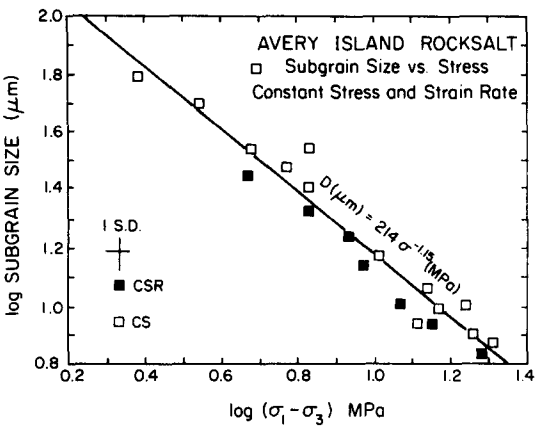

Fig. 8. Log subgrain size vs log stress plot of data obtained from constant stress (CS) and constant strain rate (CSR) steady-state tests on Avery Island salt (Table 4).

analyses of four specimens each, covering cores from the depth interval 2500–5500 feet (no depth-dependence is observed). Unidentified (classified) offshore salt structures from which sidewall (percussion) core were obtained include salt sheets, overhangs and interdomal platforms in the depth range 8000–12000 feet. Only a portion of some of the larger (3/4-inch) cores was useful because much or all of the initial substructure was overprinted by dynamic deformation (intense kinking, faulting) induced by coring; these severely distorted regions then recrystallized in a very short period. The results listed in Table 5 are plotted in Fig. 9; the diagonal line along which data points are plotted represents equation (17). Steady-state stress difference estimates range from 0.62 to 1.35 MPa, with an average near 0.9 MPa. Apart from low stress values estimated for bedded salts, there appear to be no systematic trends associated with the various tectonic environments.

Table 4. Subgrain size vs steady-state stress—$D(\mu m) = k\sigma^{-m}$ (MPa)

Rocksalt	Test type	k	$-m$	r^2	Tests	Source
Avery Island	Constant strain rate	158	1.08	0.98	7	Handin *et al.* (1986); Russell *et al.* (1990); Horseman *et al.* (1992)
Avery Island	Constant stress	226	1.14	0.92	14	Carter *et al.* (1982)
Avery Island	Constant stress + constant strain rate	214	1.15	0.91	21	Handin *et al.* (1986); Russell *et al.* (1990); Horseman *et al.* (1992)
Salina	Constant stress	166	0.88	0.84	7	Hansen (1987)
Palo Duro 4	Constant stress	273	1.29	0.91	4	Hansen (1987)
Palo Duro 5	Constant stress	133	0.71	0.45	5	Hansen (1987)
All tests	Constant stress + constant strain rate	211	1.09	0.78	37	This paper

Table 5. Rocksalt—flow stress from subgrain size—σ(MPa) = 105 $D^{-0.87}(\mu m)$

Province–structure	Mean size (μm)	1 SD (m)	$\sigma_1 - \sigma_3$ (MPa)	No. of measurements	Source
Offshore					
1.	185	4.2	1.12	444	This paper
2.	229	3.9	0.93	385	This paper
3.	266	9.8	0.81	97	This paper
4.	199	4.8	1.05	239	This paper
Coastal basins					
1. Avery Island	173	4.0	1.18	389	Carter *et al.* (1982)
1a. A.I.-85(D)	208	5.2	1.10	345	This paper
2. Barbers Hill	148		1.35		Ratigan & Vogt (in press)
3. Big Hill	262	2.4	0.82	875	This paper
4. Bryan Mound	207	2.3	1.01	835	This paper
5. W. Hackberry	192	5.7	1.08	194	This paper
Interior basins					
1. Grand Saline	330	7.1	0.67	223	Carter *et al.* (1982)
2. Keechi	249	7.8	0.86	146	This paper
3. Richton	182		1.13		Carter & Hansen (1983)
4. Vacherie	302		0.73		Carter & Hansen (1983)
Other—anticlinal (a), bedded (b)					
1. Asse (a)	221	4.4	0.96	417	Carter *et al.* (1982)
2. Cleveland (a)	185	7.1	1.12	152	Carter *et al.* (1982)
3. Lansing (a)	282	5.6	0.77	291	Carter *et al.* (1982)
4. Hutchinson (b)	312	9.1	0.71	192	This paper
5. Lyons (b)	360	10.4	0.62	120	Carter *et al.* (1982)
6. Palo Duro 4 (b)	355	21.1	0.63	58	Hansen (1987)
7. SENM (b)	338	10.0	0.66	167	Carter *et al.* (1982)

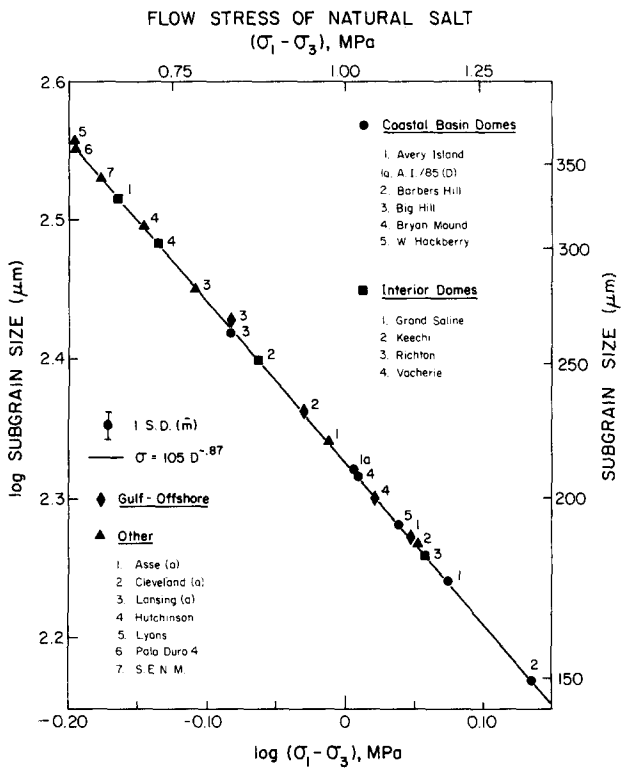

Fig. 9. Log subgrain size vs log stress showing data from natural salt structures (Table 5). Solid line shows empirical relation (equation 17) used to calculated flow stress from subgrain size.

Effect of H_2O on steady-state flow

The pronounced influence of water on ductility of halite, through crack-tip blunting and surface effects, has been discussed by Joffé (1928). Barnes (1933) suggested that plasticity of halite may be enhanced by water in fluid inclusions within crystals. To date, there have been no systematic studies of the influence of water-related point defects on dislocation mobility in halite (Carter *et al.* 1990). However, experimental and theoretical studies of crack-tip blunting and of fluid-assisted grain boundary processess have abounded in recent decades (e.g. Gorum *et al.* 1958, Stokes *et al.* 1960, Elliott 1973, Stocker & Ashby 1973, Rutter 1976, 1983, Raj 1982, Green 1984, Tada & Siever 1986, Urai *et al.* 1986, Spiers *et al*, 1989, 1990, Lehner 1990, Spiers & Schutjens 1990, Hickman & Evans 1991, Spiers & Brzesowsky 1992). These processes in rocksalt are demonstrably very important in the flow properties of salt extrusives, leading to geologically high strain rates in the range 10^{-8}–10^{-12} s^{-1} (e.g. Wenkert 1979, Talbot & Rogers 1980, Jackson & Talbot 1986), and have been influential in large-scale tectonic deformations (e.g. Heard & Rubey 1966, Talbot & Jarvis 1984). Urai *et al.* (1986, 1987) have presented evidence for operation of fluid-assisted processes in the Asse anticlinal salt and we believe that such mechanisms may be important, at least in the early stages, in the evolution of most salt structures.

In addition to recrystallization (e.g. Drury & Urai 1990), a class of fluid-assisted processes termed pressure solution is regarded as most important in limiting the creep rate. One mechanism of pressure solution has been investigated recently in a careful study by Hickman & Evans (1991, 1992) who determined the nature and rate of deformation at contacts, immersed in saturated brine, between convex lenses of halite and flat plates of halite and of fused silica. The experiments were carried out at a constant temperature of 50°C, fluid pressure of 0.1 MPa and grain contact stresses in the range 1–14 MPa. For halite–halite contacts, neck growth occurs by dendritic growth and fluid inclusion formation at the neck pore–fluid junction and this process persists throughout the experiments; convergence between the solid phases does not occur. Neck-growth, analogous to crack healing, proceeds at a rate independent of stress but dependent on crystal orientation; it appears to be driven by the reduction of interfacial energy and rate-limited either by precipitaton or diffusion in the pore fluid (Hickman & Evans 1992). However, the results of Hickman & Evans (1991) indicate that crystals forming halite–silica contacts do converge and that water-film diffusion, rate-limited either by diffusion through the intergranular pore fluid or by dissolution–precipitation kinetics, is responsible for the deformation.

Central to most models of pressure solution is that materials containing intergranular films of solvent can deform by diffusive mass transfer through the grain boundary liquid phase (Weyl 1959, Durney 1972). In these models, mass transfer, driven by stress-induced gradients in the chemical potential (e.g. Spiers & Brzesowsky in press), may be approximated by

$$\Delta\bar{\mu}_s = \sigma_n \cdot V_m, \tag{18}$$

where $\Delta\bar{\mu}_s$ is the chemical potential drop between molecule source and sink, V_m is the molar volume of the solid and σ_m is the difference in normal stress between source and sink (Paterson 1973, Raj 1982). Expressions for creep rate are then obtained from considerations of the kinetics of three serial processes—dissolution at source sites, diffusion through the grain boundary fluid and precipitation at sink sites—the slowest of which is rate-controlling for steady-state flow. Spiers *et al.* (1990) show that at low effective applied stresses (σ_e = ≤4 MPa), low volumetric strains (<15%) and temperatures in the range 20–90°C, wet NaCl aggregates (100–400 μm diameter grains) compact by this mechanism with grain boundary diffusion controlling the rate.

For these low stress and strain conditions, assuming that grain boundaries are penetrated by fluid and using Fick's first law, Spiers & Brzesowsky (in press) derive the expression

$$\dot{\beta} = \bar{A}\, V_m \cdot \frac{Z^*}{T} \cdot \frac{\sigma_e}{d^3} \cdot \frac{(1 - e_v)^{1/3}}{e_v^2}, \tag{19}$$

where $\dot{\beta}$ is the volumetric strain rate, e_v is the volumetric strain ($-\Delta V/V_o$), d is the grain diameter and A is a grain shape factor (12 ± 6). Z^* is the effective grain boundary diffusivity

$$Z^* = D_o C_o S \exp(-\Delta H/RT), \tag{20}$$

where D_o and C_o are reference diffusivity and concen-

trations (solubility), respectively, S is the thickness of the grain boundary film and ΔH is the activation enthalpy for grain boundary diffusion. Using values of Z^*, A and V_m determined by Spiers *et al.* (1990) for compaction, the constitutive relation for the creep of dense rocksalt can be written (Spiers *et al.* 1990)

$$\dot{\varepsilon}_f = 4.7 \times 10^{-4} \exp(-24.5/RT)\, \sigma/Td^3, \quad (21)$$

where the pre-exponential constant is in $mm^3\ s^{-1}$, ΔH is in kJ mol^{-1}, σ is in MPa and d is in mm.

Spiers & Brzesowsky (in press) conclude from the mechanical data and microstructural observations, that at effective stresses above 4 MPa (i.e. typically contact stresses, σ_n, near 40 MPa) plasticity-coupled pressure solution dominates and is accompanied by microfracturing, grain boundary sliding and recrystallization. Strains greater than 15% lead to constrictions of diffusion pathways and intersections of neighboring grain contacts resulting in decreases in the volumetric strain rate. Baykard & Pharr (1991) find that the presence of water at NaCl crystal contacts enhances the rate of grain boundary sliding by reducing the effective area of contact.

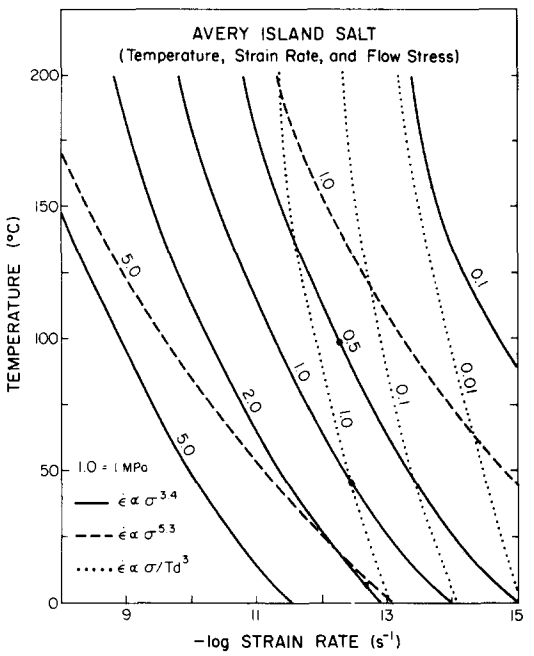

Fig. 11. −Log strain rate vs temperature plot of variations with stress of projections based on equations (12), (13) and (21) represented by solid, dashed and dotted curves, respectively. Numbers are flow stress in MPa. For any given stress and temperature, the independent mechanism giving rise to the highest strain rate will dominate; see text for discussion.

SUMMARY, DISCUSSION AND CONCLUSIONS

The foregoing summary of steady state results from constant stress and constant strain-rate tests on dry Avery Island rocksalt suggests that two flow regimes occur, each fitting a power-law relation but with different activation parameters (Fig. 7 and Table 3). This change in behavior is most readily explained by a change in rate-controlling mechanism, from cross-slip of screw dislocations in the relatively high strain-rate, high stress regime to climb of edge dislocations in the low stress, low strain-rate regime. If this rationale holds, then we may make a small adjustment to the deformation map for dry, dense aggregates of salt proposed by Munson (1979), as modified by Hansen (1987). Figure 10 shows Hansen's map with stresses and temperatures encompassed by this study indicated by the shaded block. The proposed cross-slip–climb boundary has been added. The glide–cross-slip boundary is the glide–dislocation creep boundary of Munson and the glide–climb boundary of Hansen.

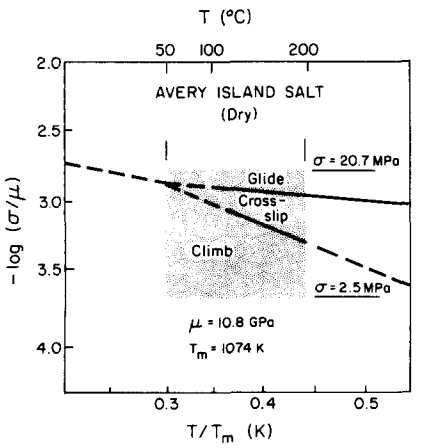

Fig. 10. Deformation map of flow processes in rocksalt (Munson 1979, Hansen 1987). Cross-slip–climb boundary from Fig. 7 is added. Stippled region shows conditions of Avery Island steady state tests.

In Fig. 11 we compare, at lower rates of natural rocksalt deformation, projections of the steady-state behavior corresponding to relations (12), (13) and (21). for independent processes, such as cross-slip (dashed curves), climb (solid curves) and fluid-assisted grain boundary diffusion (dotted curves), that giving rise to the highest creep rate will dominate the creep strain. For the comparison, we have assigned the linear stress–strain-rate relation (21) a grain diameter of 7.5 mm. Focusing on the 1.0 MPa curve for all three relations, the dashed curve lies to the right of the others at all temperatures and hence cross-slip-limited deformation should contribute little to the creep strain. Curves representing the linear ($\dot{\varepsilon} \propto \sigma/Td^3$) and climb-controlled ($\dot{\varepsilon} \propto \sigma^{3.4}$) non-linear behavior intersect at 43°C. At temperatures lower than 43°C, linear behavior should dominate whereas at higher temperature, non-linear flow gives the higher strain rate. At a stress difference of 0.5 MPa, the solid dot near 100°C on the bold 0.5 MPa curve represents the intersection of linear and non-linear response. Therefore, for temperatures lower than 100°C, fluid-assisted grain boundary diffusional creep should dominate provided that a sufficient quantity of water is available. This holds for the entire temperature range considered for stress differences <0.3 MPa for this grain size. Clearly merited are investigations of critical quantities of water required for a linear mechanical response.

The temperature-dependence of equivalent viscos-

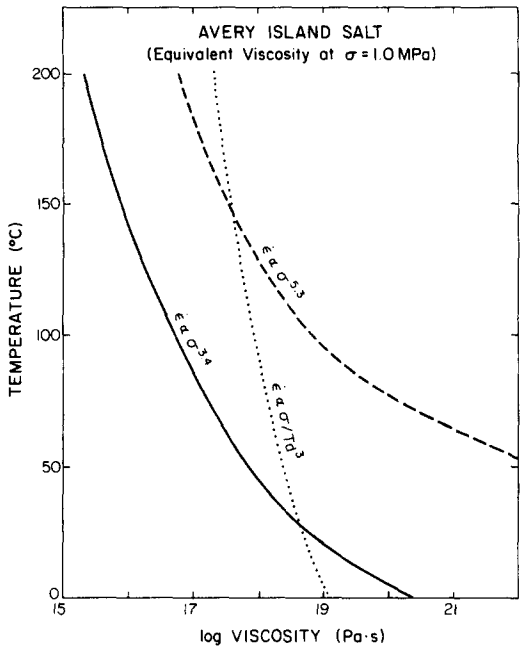

Fig. 12. Log equivalent viscosity vs temperature plot of variations in viscosity at 1 MPa stress difference predicted by equations (12), (13) and (21). Viscosities for equations (12) (solid curves) and (13) (dashed curves) are stress-dependent ($\eta = \sigma/3\dot{\varepsilon}$) while those for equations (21) (dotted curves) are not ($\eta = \sigma/\dot{\varepsilon}$).

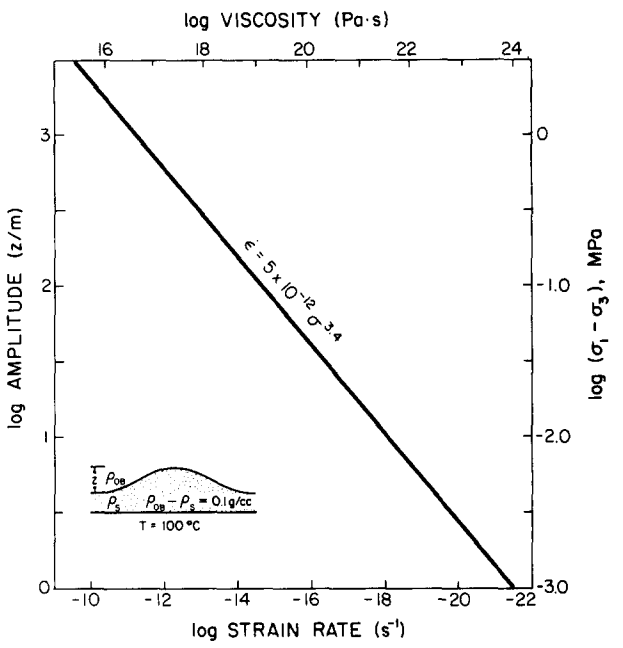

Fig. 13. Log amplitude (stress) vs log strain rate (viscosity) plot of salt pillow (stippled) growth into overburden that is 0.1 g cm^{-3} denser. Stresses are the result of buoyancy forces alone ($\Delta\sigma = \Delta\rho \cdot z \times 10^{-6}$) and corresponding strain rates are calculated from (12).

ities at 1.0 MPa stress difference predicted by the three flow equations is as shown in Fig. 12. For the two non-linear power-law relations, the climb-controlled one predicts an equivalent viscosity ($\eta = \sigma/3\dot{\varepsilon}$) lower by from 1.5 to 4 orders of magnitude over the temperature range 50–200°C. At 125°C, the viscosity is 2×10^{16} Pas, a value possibly low enough for cyclic thermal convection in thick salt layers (Jackson & Talbot 1986). At temperatures above 25°C, this non-linear relation also predicts viscosities lower than those ($\eta = \sigma/\dot{\varepsilon}$) found for the linear flow law. To illustrate the effect of grain size on the linear relation (21), doubling the grain diameter results in a decrease in creep rate and corresponding increase in viscosity by one order of magnitude, equivalent to a 10-fold reduction in differential stress.

Jackson & Talbot (1986) have provided a comprehensive discussion of salt kinematics and dynamics as they relate to salt structure evolution within various types of tectonic framework. They show that in order to initiate salt pillow growth within a time frame reasonable for tectonic evolution of the Gulf Coast, a minimum strain rate of $10^{-16}\,s^{-1}$ is required. Differential loading in sedimentary basins is suggested as the major cause for initiating pillow growth and for sustaining the asymmetry of many of the salt structures. Buoyancy alone is ruled out because forces corresponding to an initial 160 m topographic relief of the salt–sediment interface are required to provide the minimum flow rate, assuming that the Hansen & Carter (1984) flow law describes the salt behavior (Jackson & Talbot 1986). However, using the new climb-controlled flow law of Horseman *et al.* (1992), the required relief (Fig. 13) is reduced by a factor of four and thus is not so formidable. Average flow stresses recorded by subgrain size, 0.9 MPa, shed no light on the early history as stress levels of this magnitude, if produced by buoyancy alone, could reflect only those of a mature diapir that has undergone a 10^3 amplication (Fig. 13). Forces other than buoyancy must account for paleostresses in bedded salts and shallow concordant intrusions and generally, for salt diapirs, initiation by differential loading seems most plausible. Unfortunately, as for many metamorphic tectonites, information pertinent to the early stages of deformation has been obliterated by later overprinting during continuing dynamic evolution of these salt mountains.

Mazariegos & Russell (1992) and Mazariegos (1993) have made use of the climb-controlled (equation 12) and linear (equation 21) flow relations in a two-dimensional finite volume numerical analysis of the morphology and history of diapiric salt structures. Using East Texas Basin sedimentation rates (Loocke 1978, Seni & Jackson 1984) and the non-linear rheology, they find that, for a reasonable geological time frame, differential loading is effective in inducing perturbations and asymmetrical pillows that evolve to mature salt structures similar to those observed. Equivalent stresses and viscosities predicted in models using the fluid-assisted linear law are 10^2 times lower than for the climb-controlled relation and growth rates are 2.5 times higher. The nature of the mechanical constraints imposed by the overburden remains the major uncertainty in models of the evolution of salt structures but that difficult problem is now being addressed by experiments on shale (Ibanez *et al.* 1992, Ibanez & Kronenberg in press).

Acknowledgements—This research was supported by DOE/BES Award DE-FG05-87ER1371, by NATO Grant CRG 900591 and by TAMU CEMR Grant 155129. Ampara Celma, Eric Laine, Colin Peach and Tom Pfeiffle provided information and analyses important

to various aspects of the study. The manuscript benefited greatly from thorough reviews by Steve Hickman, Andreas Kronenberg, Chris Spiers and Janos Urai. We are especially indebted to Andreas Kronenberg and Chris Spiers for their active participation and counsel throughout this project.

We are very pleased to dedicate this article in honor of John Christie, an absolutely first-rate structural geologist and petrologist and, most importantly, mentor and good friend of N. L. Carter.

REFERENCES

Aubertin, M., Gill, D. E. & Ladanyi, B. 1991. A unified model for the inelastic flow of alkali halides. *Mech. Mater.* **11**, 63–82.

Barnes, R. B. 1933. The plasticity of rocksalt and its dependence upon water. *Phys. Rev.* **44**, 898–902.

Baykara, T. & Pharr, G. M. 1991. Effects of liquid phases on intrinsic interfacial sliding of alkali halide crystals. *Acta metall. Mater.* **39**, 1141–1150.

Beeman, M. L. & Kohlstedt, D. L. 1988. Dislocation density: Stress relationships in natural and synthetic sodium chloride. *Tectonophysics* **149**, 147–161.

Blum, W., Vogler, S. & Biberger, M. 1989. Stress dependence of the creep rate at constant dislocation structure. *Mater. Sci. Engng* **A112**, 93–106.

Burke, P. M. 1968; High temperature creep of polycrystalline sodium chloride. Unpublished Ph.D. thesis, Stanford University, Stanford, California.

Carter, N. L. & Hansen, F. D. 1983. Creep of rocksalt. *Tectonophysics* **92**, 275–333.

Carter, N. L. & Kirby, S. H. 1978. Transient creep and semibrittle behavior of crystalline rocks. *Pure & Appl. Geophys.* **116**, 807–839.

Carter, N. L. & Tsenn, M. C. 1987. Flow properties of continental lithosphere. *Tectonophysics* **136**, 27–63.

Carter, N. L., Hansen, F. D. & Senseny, P. E. 1982. Stress magnitudes in natural rock salt. *J. geophys. Res.* **87**, 9289–9300.

Carter, N. L., Kronenberg, A. K., Ross, J. V. & Wiltschko, D. V. 1990. Control of fluids on deformation rocks. In: *Deformation Mechanisms, Rheology and Tectonics* (edited by Knipe, R. J. & Rutter, E. H.). *Spec. Publs geol. Soc. Lond.* **54**, 1–13.

Chan, K. S., Bodner, S. R., Fossum, A. F. & Munson, D. E. 1992. A constitutive model for inelastic flow and damage evolution in solids under triaxial compression. *Mech. Mater.* **14**, 1–14.

Drury, M. R. & Urai, J. L. 1990. Deformation-related recrystallization processes. *Tectonophysics* **172**, 235–253.

Durney, D. W. 1972. Solution transfer, an important geological deformation mechanism. *Nature* **237**, 315–317.

Eargle, P. H. 1970. Regional geology and the Salmon Event. In: *Proc. Symp. Geology—Technology of Gulf Coast Salt, LSU, Baton Rouge*, 87–107.

Elliott, D. 1973. Diffusion flow laws in metamorphic rocks. *Bull. geol. Soc. Am.* **84**, 2645–2664.

Gorum, A. E., Parker, E. R. & Pask, J. A. 1958. Effect of surface conditions on room-temperature ductility of ionic crystals. *J. Am. Ceram. Soc.* **41**, 161–164.

Green, H. W., II 1984. "Pressure solution" creep: some causes and mechanisms. *J. geophys. Res.* **89**, 4313–4318.

Guillope, M. & Poirier, J. P. 1979. Dynamic recrystallization during creep of single-crystalline halite: an experimental study. *J. geophys. Res.* **84**, 5557–5567.

Handin, J., Russell, J. E. & Carter, N. L. 1986. Experimental deformation of rocksalt. In: *Mineral and Rock Deformation: Laboratory Studies* (edited by Hobbs, B. E. & Heard, H. C.). *Am. Geophys. Un. Geophys. Monogr.* **36**, 117–160.

Hansen, F. D. 1987. Physical and mechanical variability of natural rock salt. *Bull. Ass. Engng Geol.* **24**, 227–234.

Hansen, F. D. & Carter, N. L. 1984. Creep of Avery Island rocksalt. In: *Proceedings of the First Conference on Mechanical Behavior of Salt* (edited by Hardy, H. R. Jr & Langes, M. M.). Trans. Tech. Publications, Clausthal-Zellerfeld, Germany, 53–69.

Hansen, F. D. & Mellegard, K. D. 1980. Quasi-static strength and deformational characteristics of domal salt from Avery Island, Louisiana. Report prepared by RE/SPEC Inc. for Office of Nuclear Waste Isolation, ONWI-116.

Heard, H. C. & Rubey, W. W. 1966. Tectonic implications of gypsum dehydration. *Bull. geol. Soc. Am.* **77**, 741–760.

Helle, A. S. Easterling, K. E. & Ashby, M. F. 1985. Hot-isostatic pressing diagrams: new developments. *Acta Metall.* **33**, 2163–2174.

Herrmann, W. & Lauson, H. S. 1981a. Review and comparison of transient creep laws used for natural salt. Sandia Laboratories, Albuquerque. New Mexico, SAND 81-0738.

Herrmann, W. & Lauson, H. J. 1981b. Analysis of creep data for various natural rock salts. Sandia Laboratories, Albuquerque. New Mexico, SAND 81-2567.

Hickman, S. H. & Evans, B. 1991. Experimental pressure solution in halite: the effect of grain/interphase boundary structure. *J. Geol. Soc. Lond.* **148**, 549–560.

Hickman, S. H. & Evans, B. 1992. Growth of grain contacts in halite by solution-transfer: Implications for diagenesis, lithification and strength recovery. In: *Fault Mechanics and Transport Properties of Rocks*. Academic Press, London, 253–280.

Horseman, S. T. & Handin, J. 1990. Triaxial-compression tests on rocksalt at temperatures from 50 to 200°C and strain rates from 10^{-4} to 10^{-9}/s. *Am. Geophys. Un. Geophys. Monogr.* **56**, 103–110.

Horseman, S. T., Russell, J. E., Handin, J. & Carter, N. L. 1992. Slow experimental deformation of Avery Island salt. In: *Seventh International Symposium on Salt*, Vol. 1. Elsevier, Amsterdam, 67–74.

Ibanez, W. D. & Kronenberg, A. K. In press. Experimental deformation of shale: Mechanical properties and microstructural indicators of mechanisms. International Symposium on Rock Mechanics, University of Wisconsin, Madison, Wisconsin.

Ibanez, W. D., Kronenberg, A. K. & Wenk, H. R. 1992. Anisotropy and the brittle–ductile deformation of shale. (Abstract.) *Eos* **73**, Suppl. 14, 309.

Jackson, M. P. A. & Talbot, C. J. 1986. External shapes, strain rates and dynamics of salt structures. *Bull. geol. Soc. Am.* **97**, 305–323.

Jackson, M. P. A. & Talbot, C. J. 1989. Anatomy of mushroom-shaped diapirs. *J. Struct. Geol.* **11**, 1–20.

Jackson, M. P. A., Cornelius, R. R., Craig, C. H., Gansser, A., Stocklin, J. & Talbot, C. J. 1990. Salt diapirs of the Great Kavir central Iran. *Mem. geol. Soc. Am.* **177**.

Joffé, A. 1928. *The Physics of Crystals*, McGraw-Hill, New York.

Knauth, L. P. & Kumar, M. B. 1981. Trace water content of salt in Louisiana salt domes. *Science* **213**, 1005–1007.

Lehner, F. K. 1990. Thermodynamics of rock deformation by pressure solution. In: *Deformation Processes in Minerals, Ceramics and Rocks* (edited by Barber, D. J. & Meredith, P.D.). Unwin Hyman, London, 296–333.

Loocke, J. E. 1978. Growth history of the Hainesville salt dome, Wood County, Texas. Unpublished Master's thesis, University of Texas at Austin.

Mazariegos, R. A. 1993. Mechanical modeling of the growth of salt structures. Unpublished Ph.D. dissertation, Texas A&M University.

Mazariegos, R. A. & Russell, J. E. 1992. Growth of diapiric salt structures: integration of experimental and numerical work. (Abstract.) *Eos* **73**, 572.

Mendelson, S. 1961. Dislocation etch formation in sodium chloride. *J. appl. Phys.* **32**, 1579–1582.

Munson, D. E. 1979. Preliminary deformation-mechanism map for salt. Sandia Laboratories, Albuquerque, New Mexico, SAND 79-0076.

Munson, D. E. & Dawson, P. R. 1984. Salt constitutive modeling using mechanism maps. In: *Proceedings of the Second Conference on Mechanical Behavior of Salt* (edited by Hardy, H. R., Jr and Langer, M. N.). Trans. Tech. Publications, Hanover, Germany, 717–737.

Paterson, M. S. 1973. Non-hydrostatic thermodyamics and its geological applications. *Rev. Geophys. & Space Phys.* **11**, 355–389.

Peach, C. J. 1991. Influence of deformation on the fluid transport properties of salt rocks. Ph.D. dissertation, University of Utrecht, The Netherlands (*Geologica Ultraiectina* **77**).

Poirier, J. P. 1972. High temperature creep of single-crystal sodium chloride. *Phil. Mag.* **26**, 713–725.

Poirier, J. P. 1985. *Creep of Crystals*. Cambridge University Press, New York.

Raj, R. 1982. Creep in polycrystalline aggregates by matter transport through a liquid phase. *J. geophys. Res.* **87**, 4731–4739.

Raleigh, C. B. & Kirby, S. H. 1970. Creep in the upper mantle. *Spec. Pap. Miner. Soc. Am.* **3**, 113–121.

Ratigan, J. L. & Vogt, T. J. In press. LPG storage at Mont Belvieu, Texas: A case history. *Soc. Petrol. Engng.*

Ratigan, J. L., VanSambeek, L. L., De Vries, K. L. & Nieland, J. D. 1992. The influence of seal design on the development of the disturbed rock zone. Topical Rep. RSI-0400, RE/SPEC Inc., Rapid City, South Dakota.

Russell, J. E., Carter, N. L. & Walker, S. C. 1990. A material model

for Avery Island Rocksalt. *Am. Geophys. Un. Geophys. Monog.* **56**, 111–118.
Rutter, E. H. 1976. The kinetics of rock deformation by pressure solution. *Phil. Trans. R. Soc.* **A283**, 203–219.
Rutter, E. H. 1983. Pressure solution in nature, theory and experiment. *J. geol. Soc. Lond.* **140**, 725–740.
Seni, S. J. & Jackson, M. P. A. 1984. Sedimentary record of Cretaceous and Tertiary salt movement, East Texas Basin. Bureau of Economic Geology, Report 139, Austin.
Seni, S. J. 1991. Evolution of stocks and massifs from burial of salt sheets on the continental slope, north Gulf of Mexico. Unpublished Ph.D. dissertation, University of Texas, Austin.
Senseny, P. E. 1988. Creep properties of four salt rocks. In: *Proceedings of Second Conference on Mechanical Behavior of Salt* (edited by Hardy, H. R., Jr & Langer, M. N.). Trans. Tech. Publications, Hanover, Germany 431–444.
Senseny, P. E., Hansen, F. D., Russell, J. E., Carter, N. L. & Handin, J. 1992. Mechanical behavior of rock salt: Phenomenology and micromechanisms. *Int. J. Rock Mech.* **29**, 363–378.
Servi, I. S. & Grant, N. D. 1951. Structure observations of aluminum deformed in creep at elevated temperature. *Trans. A.I.M.E.* **191**, 917–922.
Simmons, G. R. 1992. The regional distribution of salt in the northwestern Gulf of Mexico: Styles of emplacement and implications for early tectonic history. Unpublished Ph.D. dissertation, Texas A&M University, Texas.
Skrotski, W. & Haasen, P. 1988. The role of cross slip in the steady state creep of salt. In: *Proceedings of Second Conference on Mechanical Behavior of Salt* (edited by Hardy, H. R., Jr & Langer, M. N.). Trans. Tech. Publications, Hanover, Germany, 69–81.
Spiers, C. J. & Brzesowsky, R. H. In press. Densification behavior of wet granular salt: Theory versus experiment. 7th International Symposium on Salt.
Spiers, C. J., Peach, C. J., Brzesowsky, R. H., Schutjens, P. M. T. M., Liezenberg, J. L. & Zwart, H. J. 1989. Long-term rheological and transport properties of dry and wet salt rocks. Nuclear Science and Technology, EUR 11848 EN. Office for Official Publications of the European Communities, Luxembourg.
Spiers, C. J., Peach, C. J. & Celma, A. G. 1986. Long-term rheological and transport properties of dry and wet salt rocks. First Periodic. Rep. contract F1 1W-0051-NL, University of Utrecht, The Netherlands.
Spiers, C. J. & Schutjens, P. M. T. M. 1990. Densification of crystalline aggregates by fluid-phase diffusional creep. In: *Deformation Processes in Minerals, Ceramics and Rocks* (edited by Barber, D. J. & Meredith, D. D.). Unwin Hyman, London, 334–353.
Spiers, C. J., Schutjens, P. M. T. M., Brzesowsky, R. H., Peach, C. J., Liezenberg, J. L. & Zwart. H. J. 1990. Experimental determination of constitutive parameters governing creep of rocksalt by pressure solution. In: *Deformation Mechanisms, Rheology and Tectonics* (edited by Knipe, R. J. & Rutter, E. H.). *Spec. Publs geol. Soc. Lond.* **54**, 215–227.
Stocker, R. L. & Ashby, M. F. 1973. On the rheology of the upper mantle. *Rev. Geophys. & Space Phys.* **11**, 391–426.
Stokes, R. J., Johnson, T. L. & Li, C. H. 1960. Environmental effects on the mechanical properties of ionic solids with particular reference to the Joffé effect. *Trans. metall. Soc. A.I.M.E.* **218**, 655–662.
Stolper, E. 1982. Water in silicate glasses: an infrared spectroscopic study. *Contr. Miner. Petrol.* **81**, 1–17.
Stone, D. S. 1991. Scaling laws in dislocation creep. *Acta metall. Mater.* **39**, 599–608.
Stormont, J. C., Howard, C. L. & Daemen, J. J. K. 1991. Changes in rock salt permeability due to nearby excacavation. In: *Proc. 32nd U.S. Symposium, Rock Mechanics as Multidisciplinary Science* (edited by Rogiers, J. C.). Balkema, Rotterdam, The Netherlands, 899–907.
Tada, R. & Siever, R. 1986. Experimental knife-edge pressure solution of halite. *Geochim. cosmochin. Acta* **50**, 29–36.
Takeuchi, S. & Argon, A. S. 1976. Steady-state creep of single phase crystalline matter at high temperature. *J. Mater. Sci.* **11**, 1542–1566.
Talbot, C. J. & Jackson, M. P. A. 1987. Internal kinematics of salt diapirs. *Bull. Am. Ass. Petrol. Geol.* **71**, 1068–1093.
Talbot, C. J. & Jarvis, R. J. 1984. Age, budget and dynamics of active salt extrusions in Iran. *J. Struct. Geol.* **6**, 521–533.
Talbot, C. J. & Rogers, E. A. 1980. Seasonal movements in salt glacier in Iran. *Science* **208**, 395–391.
Urai, J. L., Spiers, C. J., Hendrik, H. J., Zwart, H. J. & Lister, G. S. 1986. Weakening of rock-salt by water during long-term creep. *Nature* **324**, 554–557.
Urai, J. L., Spiers, C. J., Peach, C. J., Franssen, R. C. M. W. & Liezenberg, J. L. 1987. Deformation mechanisms operating in naturally deformed halite rocks as deduced from microstructural investigations. *Geologie Mijnb* **66**, 164–176.
Vendeville, B. C. & Jackson, M. P. A. 1992. The rise and fall of diapirs during thin-skinned extension. *Bur. Econ. Geol. Rep.* **209**.
Vendeville, B. C. & Jackson, M. P. A. In press. The rise of diapirs during thin-skinned extension. *Mar. Petrol. Geol.*
Wawersik, W. R. 1988. Alternatives to a power-law creep model for rock salt at temperatures below 160°C. In: *Proceedings of Second Conference on Mechanical Behavior of Salt* (edited by Hardy, H. R., Jr & Langer, M. N.). Trans. Tech. Publications, Hanover, Germany, 103–128.
Wawersik, W. R. & Zeuch, D. H. 1986. Modelling and mechanistic interpretation of creep of rocksalt below 200°C. *Tectonophysics* **121**, 125–152.
Webster, G. A., Cox, A. P. D. & Dorn, J. E. 1969. A relationship between transient and steady-state creep at elevated temperatures. *Metal Sci. J.* **3**, 221–225.
Weertman, J. & Weertman, J. R. 1970. Mechanical properties, strongly temperature dependent. In: *Physical Metallurgy* (edited by Cahn, R. W.). Elsevier, New York, 983–1010.
Wenkert, D. D. 1979. The flow of salt glaciers. *Geophys. Res. Lett.* **6**, 523–526.
Weyl, P. K. 1959. Pressure solution and the force of crystallization—a phenomenological theory. *J. geophys. Res.* **64**, 2005–2025.
Worrall, D. M. & Snelson, S. 1989. Evolution of the northern Gulf of Mexico with emphasis on Cenozoic growth faulting and the role of salt. In: *The Geology of North America—An Overview. Bull. geol. Soc. Am.* **A**, 97–138.